Conference Proceedings

EuroSun 2016
Palma de Mallorca (Spain), 11 - 14 October 2016

Holographic photovoltaic-thermal module for window louvre integration: Design and simulation

Alex Moreno[1], Julia Marín-Sáez[1], Alberto Riverola[1], Daniel Chemisana[1], Jesús Atencia[2], María Victoria Collados[2]

[1] University of Lleida, Lleida (Spain)

[2] University of Zaragoza, Zaragoza (Spain)

Abstract

A building integrated holographic concentrating photovoltaic-thermal system has been optically and energetically simulated. The system has been designed to be superimposed into a solar shading louvre; in this way the concentrating unit takes profit of the solar altitude tracking, which the shading blinds already have, to increase system performance. An energetic simulation has been conducted for Avignon (France), which is a European representative location suitable for solar applications with available atmospheric parameter and irradiance experimental data sets. The simulation tool utilized has been TRNSYS, coupled with MATLAB (where the ray-tracing algorithm to simulate the holographic optical performance has been implemented). In the frame of the simulation, a comparison with a conventional photovoltaic-thermal (PVT) module installed on the blinds and with the same area than the concentrator aperture one is conducted. The concentrator achieves an annual mean optical efficiency of 43.0%, an electrical energy production of 148.2 kWh/kWp and a thermal energy of 250.4 kWh/m^2. On the other hand, the reference PVT module behaves very similar in terms of the thermal energy yielding 294.2 kWh/m^2 but almost doubles the electrical annual production with 281.7 kWh/kWp.

Keywords: *solar energy, solar concentration, photovoltaics, PVT, holographic optical elements (HOE), building integration, energy dynamic simulation.*

1. Introduction

Energy consumption in the building sector represents 40% of the total energy consumed in the European Union. The European Commission, in order to decrease energy consumption, defined (considering buildings as a priority) the directive which states the "20-20-20" objectives: greenhouse gas emissions reductions (20%), the share of renewable energy (20%) and improvements in energy efficiency (20%) (*Directive 2010/31/EU of the European Parliament and of the Council of 19 May 2010 on the energy performance of buildings.*, 2010). In this regard, building integrated solar hybrid Concentrating Photovoltaic-Thermal (CPVT) systems are a technology which perfectly addresses the objectives defined by the European Union, as may cover both the thermal and the electrical consumption needs.

CPV systems replace part of the cell area by cheaper and more environmentally friendly materials, the optical elements, which can lead to more cost-efficient systems from both, economic and environmental aspects (Menoufi et al., 2013). On the contrary, when increasing the concentration ratio the percentage which is not converted into electricity becomes much higher in absolute terms. This could cause PV overheating and thus, problems related with efficiency reduction, stress of materials, etc. arise. A strategy to profit the removal heat which negatively influences system performance is to use a hybrid Photovoltaic-Thermal (PVT) receptor. A PVT module controls PV temperature while simultaneously produces thermal energy. Another strategy to prevent the PV warming up is the spectral selection of the incident irradiance. A technology able to concentrate sunlight and at the same time to spectrally select irradiance is holography.

Among the different types of Holographic Optical Elements (HOEs), volume holograms have been studied as solar concentrators attending to some interesting properties as the high optical efficiency achieved (they can reach 100% efficiency for a selected wavelength). They may be utilized in different configurations (Collados et

doi:10.18086/eurosun.2016.08.03 Available at http://proceedings.ises.org

al., 2016): plane gratings, that are not concentrating elements but as they operate directing light toward the same area the incident irradiance is concentrated (Castillo, 2011; Castro et al., 2010; Zhang et al., 2011) or concentrating optical elements (lenses) either cylindrical (Chemisana et al., 2013; Ludman et al., 1997) or spherical (Ludman, 1982; Vorndran et al., 2015; Zhang et al., 2013).

HOEs present two main characteristics that affect their performance: angular and chromatic selectivity, in other words, their efficiency depends on the angle of incidence and the wavelength. Consequently, the solar spectrum and the spectral sensitivity range of the photovoltaic cell, among other parameters, need to be taken into account in the design of the HOE, in order to optimize its behavior for the wavelength range of interest. The chromatic selectivity of holograms provides an important advantage in comparison with refractive elements, since the concentration of undesired wavelengths on the photovoltaic cell is avoided. If the HOE is designed to diffract infrared wavelengths with very poor efficiency, the cell is prevented from overheating, which could cause a worsening on the cell's performance (Chander et al., 2015; Xiao et al., 2014). The chromatic selectivity also allows spectrum splitting, if a configuration with more than one kind of receiver (either different photovoltaic cells (Ludman et al., 1997; Zhang et al., 2013) or a hybrid photovoltaic-thermal receiver (Froehlich et al., 1993; Iurevych et al., 2012; Vorndran et al., 2015; Xia et al., 2011)) is chosen.

More specifically, regarding holographic PVT designs: Vorndran et. al. (Vorndran et al., 2015) proposed a spectrum-splitting holographic system in which a holographic lens diffracts a narrow bandwidth towards a photovoltaic cell. The transmitted spectrum is reflected on a parabolic mirror towards a thermal tube. The solar concentrator described by Froehlich et. al. (Froehlich et al., 1993) is formed by two stacked holographic lenses, each composed by a holographic grating to correct the incident direction and a holographic lens. Each holographic lens directs a different spectral range of the incoming light to a photovoltaic cell, sensitive to one of these two spectral bandwidths. The transmitted spectrum reaches a thermal absorber, which also refrigerates the PVs. Xia et. al. (Xia et al., 2011) proposed a solar concentrator formed by a holographic grating, which would split the incident spectrum into visible and infrared range, and a Fresnel lens, which would concentrate the visible spectrum onto a set of PV cells and the IR spectrum onto a heat exchanger. Iurevych et. al. (Iurevych et al., 2012) simulated the performance of a solar concentrator constituted by a reflection holographic grating. Incoming rays with wavelengths of a certain range are reflected by the HOE and the surfaces of the system, reaching a PV cell, whereas the rest are transmitted through the HOE and reach a thermal absorber.

Based on the previous studies found in the literature, it can be noted that even though there are some works conducting optical and energetic simulation of holographic concentrators, there is no research dealing with the energy simulation of the system performance in a building integrated configuration. In this regard, the present research is the continuation of that presented by the authors in (Marín-Sáez et al., 2016b) and aims at covering an important gap in the frame of Holographic Concentrating Photovoltaic-Thermal (HCPVT) solar generators, which is their dynamic energy simulation. For this purpose, the electrical and thermal energy productions of the proposed HCPVT are simulated and compared with those obtained by a conventional reference PVT system.

2. System description

The analyzed building integrated concentrating PVT system is designed to be superimposed on the blinds of a solar louvre shading system. In this manner, the concentrator is benefitted from the solar altitude tracking of the shading blinds and thus increasing the optical efficiency. Figure 1 illustrates the architectural configuration proposed, indicating in light blue the blind area where the concentrating system is placed (top-left). The blinds' size is 9 meters long by 0.4 meters wide and by 0.065 m high. The simulated building is considered to be 5.8 m height, starting the blinds at the ground floor window level (1 m height), therefore the number of blinds is 12. On the top-right, a schematic of a blind section shows the location of the holographic lenses and the PVT module, which is placed in the interior space. Both elements are assembled in a single unit forming a modular system with two parallel layers, the HOEs and the PVT module. At the bottom, a diagram of the cross section indicates the main dimensions of the module.

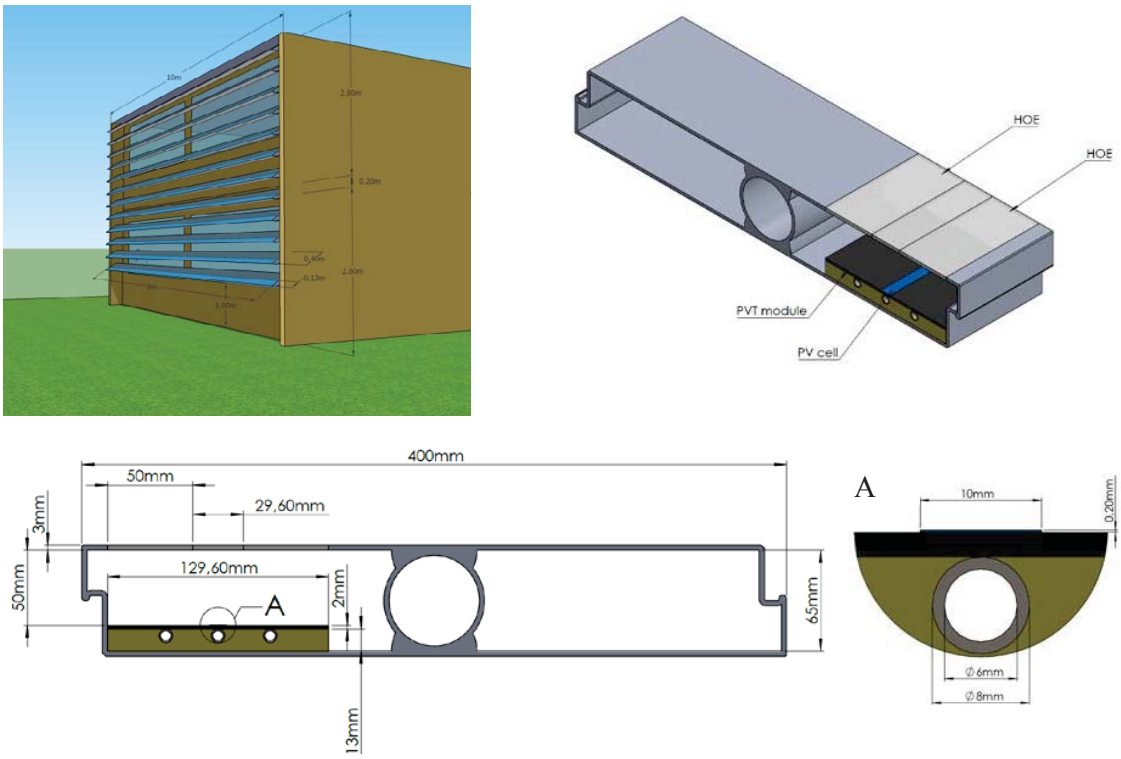

Figure 1. Architectural image of the building integrated concentrator (top-left), section of the blind where the PVT concentrator in placed (top-right) and cross-section and detail of the blind with the PVT concentrator (bottom). (Marín-Sáez et al., 2016b)

The concentrating system consists of two holographic lenses that focus incident irradiance toward the PVT module. Both lenses are attached to the same glass substrate, which at the same time closes the space between them. In figure 2a, a diagram of the ray-tracing is represented. Three different wavelengths in the range of maximum spectral response of the Si PV cell are depicted to show the rays' spatial distribution at the *YZ* plane.

2.1. Holographic optical element

A cylindrical holographic lens is chosen as a solar concentrator HOE. The recording of such lens is carried out by means of the interference of a plane wave and a cylindrical wave onto a photosensitive medium, as shown in Figure 2b. This turns into variations of the refraction index along the material.

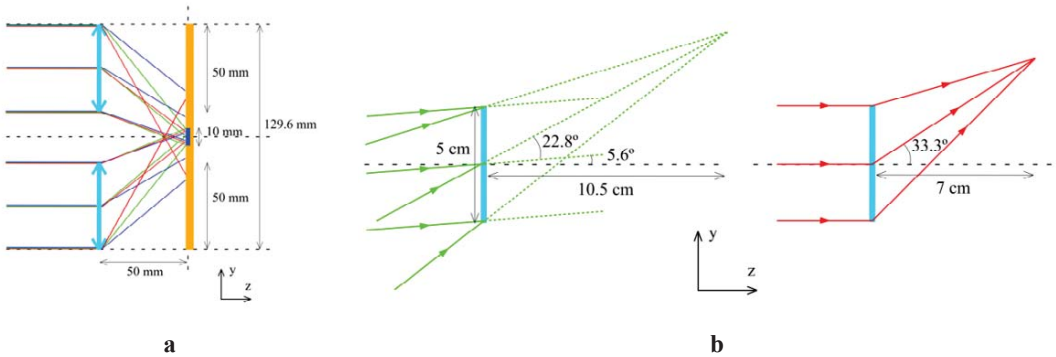

Figure 2. a) Schematic of the HCPVT generation unit (right), with ray-tracing for rays with three different wavelengths: 700 (depicted with blue lines), 800 (green lines) and 900 nm (red lines); b) Sketch of the recording (center, at 532 nm) and reconstruction (right, at 800 nm) schemes of the holographic cylindrical lens simulated in this study. (Marín-Sáez et al., 2016b)

When illuminating a volume hologram at the reconstruction stage, only two waves are found at its output: the transmitted wave and the diffracted wave. With the adequate incident conditions (wavelength and angle), the efficiency of the diffracted beam is maximal, and it can reach 100 % for a selected wavelength if the design is also optimum. When illuminating a holographic cylindrical lens with a plane wave, the resulting diffracted wave is a cylindrical one, as it is shown in Figure 2b.

The reconstruction wavelength for which the HOE will be most efficient is set at 800 nm. This value results from a compromise between the incident solar spectrum (with maximal intensity at wavelengths around 500-800 nm most of the day) and the photovoltaic cell sensitivity (optimum around 700-1000 nm for mono-Si cells). Incident light at 800 nm will focus at a line parallel to the x-axis, 7 cm away from the HOE, as it is shown in Figure 2b. However, the PVT module is placed at 5 cm away from the HOE, in order to collect more energy of the desired wavelength range, since rays with different wavelengths are led towards different directions, as it is illustrated in Figure 2a.

Holograms present higher angular selectivity when the incidence direction varies in the plane formed by the two recording beams, and lower in the perpendicular plane. Taking advantage of this effect, a cylindrical lens offers the possibility of suppressing tracking in one direction. Therefore, tracking is only necessary along the direction with higher angular selectivity.

The proposed recording material of the HOE is Bayfol HX, a photopolymer manufactured by Covestro AG (Berneth et al., 2014), adequate for holographic recording with solar photovoltaic applications (Marín-Sáez et al., 2016a).

In the configuration chosen for this study, two HOEs are placed separated in the same *XY*-plane, so that the spatial distributions of the diffracted beams are symmetrical. A glass plate located in this plane serves as a substrate for the photopolymer, covers the space between the two HOEs and is assumed to have the same refractive index as the photopolymer. The distance between the two lenses, and therefore, the position of the PV cell in the y-axis, was optimized so that it would receive more energy at the most favourable wavelength range for the cell. The ratio between the x dimension of the HOEs and the PV cell was chosen to avoid vignetting on the cell of its optimal wavelength range (700 - 1000 nm).

2.2. Hybrid photovoltaic-thermal module

The PVT module units for the holographic system are considered to be 100 cm long by 12.96 cm wide; thus every shading blind of 9 m is composed of 9 PVT modules. Every PVT module is formed by 7 cells connected in series of 14.29 cm long by 1 cm wide each. The photovoltaic cells considered in the simulation are based on commercial mono-crystalline cells by Sunways ("Sunways," n.d.), whose main electrical characteristics are summed up in table 1. The characteristics of the thermal receiver are detailed in section 3.2.

In the case of the reference PVT module, it presents the same dimensions as the HCPVT one and is considered to be composed of the same type of cells (table 1) and with the same thermal receiver characteristics. The difference between both is that the reference PVT module is placed at the same position than the optical system, thus receiving the same incident irradiance.

Table 1. Parameters of the PV cells ("Sunways," n.d.).

V_{OC} [1] (V)	J_{SC} (A/m^2)	FF (%)	γ (%/°C)	T_{NOCT} (°C)
0.635	377.6	78.4	-0.44	45

[1] V_{OC} = Open circuit potential; J_{SC} = Short circuit current density; FF = Fill factor; γ = Power temperature dependence losses; T_{NOCT} = Nominal operating cell temperature.

3. Methodology

3.1. Spectra simulation

The direct normal irradiance spectrum is calculated with the SMARTS radiative model (Gueymard, 2001), whose main atmospheric input parameters are (listed by order of importance): Air mass (AM), aerosol optical depth (τ), precipitable water (PW) and Ångström exponent (α).

Measured values of Z , τ , PW and α, can be obtained from the Aerosol Robotic Network (AERONET) database ("Aerosol Robotic Network (AERONET)," n.d.). For this study, only AERONET's level 2.0 data are used to guarantee the highest possible data quality (after cloud screening, calibration and degradation correction (Holben et al., 1998)).

Detailed information on the sunlight spectrum is required for at least a complete year in order to accurately estimate the energy output of the PVT modules. Therefore, a preliminary search on AERONET's database has been done to select only those locations and years with a high density of atmospheric retrievals. These retrievals

are performed at least every 15 minutes for AM less than 5. Following the procedure described by Chan et al. (Chan et al., 2014), measurement gaps longer than 15 minutes are considered to be caused by extended cloudiness, not computing this time for the annual yield. In addition, the selected locations should be suitable for CPVT systems and have a high direct normal irradiance (DNI).

The location has been selected according to two criteria: (i) It should provide high-quality data over an extended period of time (a constraint satisfied by only a small fraction of AERONET sites); and (ii) it should have co-located and simultaneous DNI measurements, in order to validate the simulated spectra. Based on the above criteria, Avignon, France, (2003) has been chosen.

Table 2. Characteristic parameters for Avignon.

Location	Simulated year	Lat. (°)	Long. (°)	Elevation (m)	Mean daily DNI (kWh/m^2/day) [25]	Annual mean atmospheric parameters AM | τ | PW | α
Avignon	2003	43.93	4.88	32	5-5.5	2.16 | 0.25 |1.76 | 1.37

Figure 3a illustrates the monthly variation of the most representative atmospheric parameters obtained by AERONET at the selected location. This graph conveniently displays the amplitude with which each variable varies throughout the simulation year.

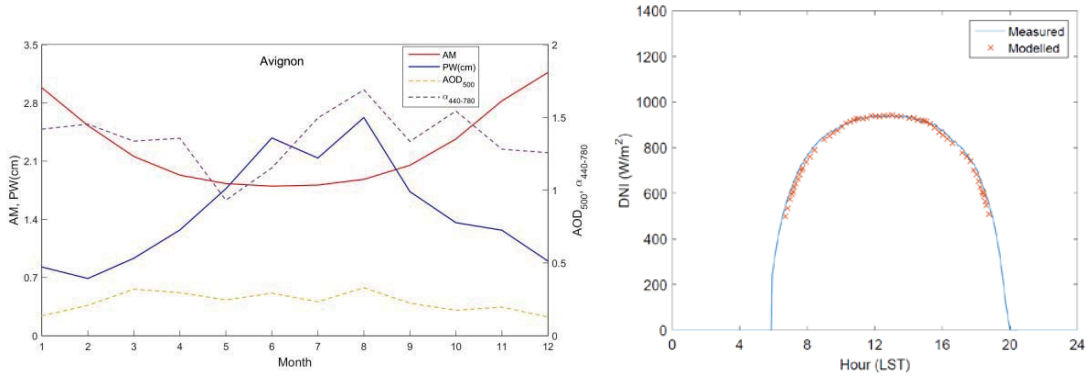

a b

Figure 3. a) Monthly-average values of the main atmospheric variables for the simulated sites, obtained from AERONET. In the case of AM, the values are limited to AM < 5, in agreement with AERONET measurements; b) DNI data validation on the 1st of August in the selected simulated year. LST: Local standard time. (Marín-Sáez et al., 2016b).

Finally, the validation of the spectra generated by SMARTS is undertaken by comparing the calculated broadband DNI to reference irradiance measurements obtained from the Baseline Surface Radiation Network (BSRN) ("World Radiation Monitoring Center – Baseline Surface Radiation Network homepage.," n.d.). A good agreement is achieved between the simulated and the measured data, as depicted in Figure 3b, showing the irradiance profiles for a cloudless typical day. The validation has been conducted using DNI data from BSRN station in Carpentras, located 28 km away.

3.2. Optical simulation

The performance analysis of the holographic lens is based on Kogelnik's Coupled Wave Theory (Kogelnik, 1969) and the approximate scalar theory established by Syms (Syms, 1985). A ray-tracing algorithm has been developed (Bañares-Palacios et al., 2015), which allows the calculation of the output directional cosines and the spectral energy associated with each ray, for the transmitted and the diffracted wave delivered to the PVT module.

The propagation wave vectors of the recording beams, $\vec{k}_1$ and, $\vec{k}_2$ with modulus $k_1 = k_2 = \frac{2\pi}{\lambda_R}$ (where λ_R is the recording wavelength), determine the grating vector $\vec{K} = \vec{k}_1 \pm \vec{k}_2$, illustrated in Figure 6. Since one of the recording beams is a cylindrical wave, its propagation wave vector has a different direction at each point along the *y*-direction, and the angle between beams is also different. Therefore, the vector $\vec{K}$, which is perpendicular

to the planes with constant refractive index variation, is spatially dependant. Its modulus is $\frac{2\pi}{\lambda}$, where Λ is the spatial period of a grating with vector $\vec{K}$, and also different at each point. Each point of the holographic lens behaves differently; thus, each point is treated as a local holographic grating.

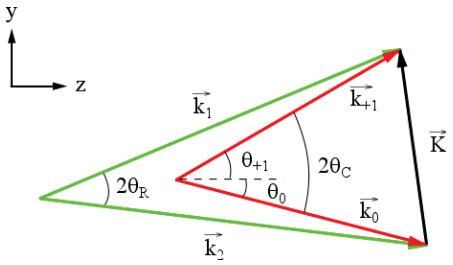

Figure 4. Sketch of the relation between the grating vector $\vec{K}$ and the wave vectors of the two recording beams, $\vec{k}_1$ and $\vec{k}_2$, and the transmitted and diffracted waves, $\vec{k}_0$ and $\vec{k}_{+1}$.

When illuminating the HOE with a wave with vector $\vec{k}_0$ and a certain wavelength λ_C, the resulting diffracted wave has a vector $\vec{k}_{+1}$, which has the same modulus as $\vec{k}_0$ and direction determined with $\vec{k}_0$ and $\vec{K}$. This relation is shown in Figure 4. Thus, if the vector $\vec{K}$ along the hologram is known, the direction of the diffracted ray originated with each incident reconstruction ray at a certain point can be calculated.

The energy of the diffracted wave from each point is calculated with equation 1:

$$\eta = \frac{\sin^2\left[\left(\nu^2 + \xi^2\right)^{1/2}\right]}{1 + \frac{\xi^2}{\nu^2}} \tag{1}$$

The parameters ν and ξ are given by:

$$\nu = \frac{\pi d \Delta n}{\lambda_C c_0 c_{+1}} \tag{2}$$

$$\xi = \frac{d\vartheta}{2c_{+1}}, \tag{3}$$

where d is the thickness of the recording material, Δn is the refraction index modulation, λ_C is the reconstruction wavelength, and c_0 and c_{+1} are the directional cosines with respect to the z-axis of the reconstruction and diffracted wave, respectively. ϑ is a parameter that determines the variation from Bragg's law, that is, the condition of maximal efficiency. Bragg's law is met when the next equation is fulfilled:

$$2\Lambda \sin\theta_C = \lambda_C, \tag{4}$$

where θ_C is the semiangle between the transmitted and the diffracted beam, shown in Figure 6. When Bragg's condition is not fulfilled the efficiency of the diffracted wave decreases, and the efficiency of the transmitted wave increases.

The energy of the transmitted wave is calculated as the remaining available energy that is not taken by the diffracted wave, at each point and for each reconstruction wavelength.

The rays entering the system through the glass plate between the two HOEs are also considered.

The simulation considers direct normal irradiance solar spectrum, generated by SMARTS, as the incident irradiance input parameter. Nevertheless, due to the implicit difficulty and computational time required, the solar semiangle and the diffuse irradiance fraction are not considered at this stage. Further research will be conducted to define the algorithm containing the particular angles of incidence and polarization constraints of the diffuse radiation, jointly with the implementation of the solar semiangle. Therefore, it should be taken into account that the irradiance delivered by the holographic concentrator is underestimated in a percentage proportional to the diffuse fraction. Losses due to Fresnel reflections on the surface and to total internal

reflection (Hecht, 1998) are taken into account in the simulations.

3.3. Energetic simulation

The energetic simulation is conducted in TRNSYS, evaluating the HCPVT performance under the weather conditions of Avignon. Figure 5 charts the monthly cumulated DNI values and the monthly average ambient temperatures. The annual cumulated DNI is 1860 kWh/m^2 and the annual mean temperature is 14.7 °C. It should be noticed that, in agreement with AERONET criteria, values with AM > 5 (solar altitude below 11.5°) are not considered and, taking into consideration the optical efficiency limitations of the concentrating system, the direct beam irradiances accepted by the HCPVT module will be significantly lower than the DNI values. Results regarding optical efficiencies are included in section 4.

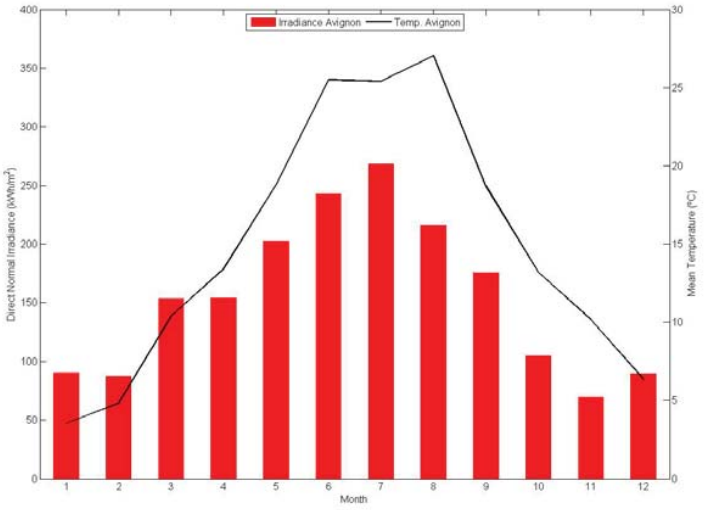

Figure 5. Monthly cumulated DNI and mean temperature values.

The optical simulation program described in subsection 3.2, which is programmed in MATLAB, is linked to TRNSYS delivering at every time step (1 minute) the irradiance impacting on the PVT module. From the irradiance received on the module, the thermal energy produced is calculated by a MATLAB code which determines the electrical power (P'_{mpp}) coupled with the thermal generator *type 1b*, as a function of the solar cell electrical parameters and the cell temperature, calculated with the following equation (5) (Marion, 2002). In the case of the reference module, the simulation is conducted in the same way but with no optical simulation.

$$P'_{mpp} = P_{mpp}\left[1+\gamma\left(T_{cell}-25\right)\right], \tag{5}$$

where P_{mpp} is the electrical power generated by a PV cell without taking into account losses due to the temperature, γ is a temperature coefficient equal to -0.44 %/°C for the PV cells considered in this study, and T_{cell} is the temperature of the cell in °C. The temperature of the cell of the PVT module is estimated with equation 6 (Amrizal et al., 2013):

$$T_{cell} = T_{in} + \frac{P_{th}}{F'U_L A}\left(1-F'\right), \tag{6}$$

where T_{in} is the input temperature of the water circulating at each module, P_{th} is the power generated by the thermal absorber, F' is the collector efficiency factor, U_L is the overall convective heat loss coefficient of the collector and A is the surface of the collector. T_{in} and P_{th} values are obtained from the previous time step, considering the error to be minimum.

The electrical power of the cell P_{mpp} without temperature effects is calculated with:

$$P_{mpp} = J_{SC}V_{OC}FF \tag{7}$$

The short circuit current, J_{SC} is calculated taking into account the spectral response curve of the mono-crystalline silicon solar cell manufacturer. The values of the open circuit voltage V_{OC} and the fill factor FF are assigned from the technical characteristics of the simulated solar cells (see Table 1).

Table 3. Parameters of the thermal collector [33].

η_0 [2] (%)	U_L (W/m^{2}K)	k_2 (W/m^{2}K^2)	$F' = \eta_0 / \tau\alpha$	ε (%)	α (%)	τ (%)
79.9	3.97	0.016	0.913	5.0	95.5	91.6

[2] η_0 = Efficiency; U_L, k_2 = Coefficients of heat loss; ε = Emission; α = Absorption; τ = Transmission and F' = Collector efficiency factor ($F' = \eta_0 / \tau\alpha$).

4. Results

The optical efficiency of the concentrating holographic system is defined in Eq. (8) as the ratio between the irradiance received at the generator surface, differentiated in the area where the PV is situated (A_{PV}) and the rest of the area where it is the thermal absorber (A_T), and the irradiance at the entrance pupil area of the system (A_E). The irradiances on the PV, thermal absorber and entrance pupil are respectively I_{PV}, I_T and I_E.

$$\eta_{opt} = \frac{I_{PV} A_{PV} + I_T A_T}{I_E A_E} . \tag{8}$$

The average optical efficiency obtained each month is presented in Figure 6. The fact that the system works better during the winter months than the summer months may seem counterintuitive. However, it is due to the lack of tracking of the system in the azimuth direction, since the maximum optical efficiency is reached when the azimuth angle, φ, is zero (at solar noon), and decreases when the absolute value of this angle increases. The azimuth angle reaches greater values in summer; therefore, the optimum incident angle range is found during less time each day, which results in lower optical efficiency, because of the angular selectivity of the HOEs.

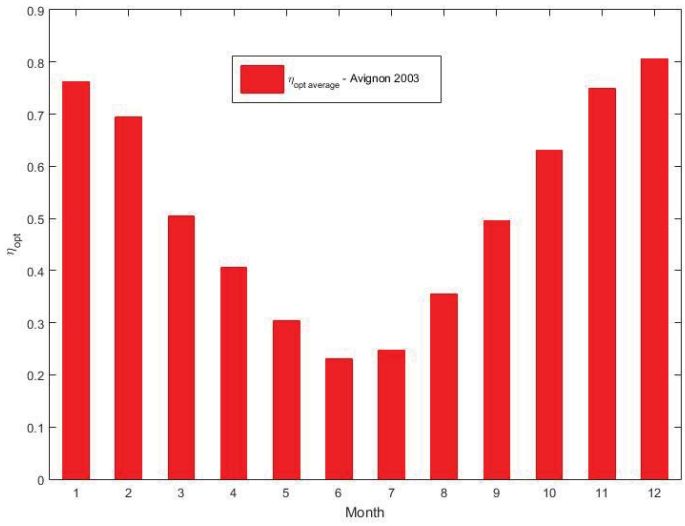

Figure 6. Average optical efficiency of the concentrating holographic system obtained each month with incident radiation of Avignon (2003).

The incident mean annual spectral irradiance received at the surface of the PV cell and at the surface of the thermal absorber, determined by means of the optical simulation described in section 3.2, is plotted in Figure 7, together with the incident solar spectral irradiance received at the entrance of the system. One of the most remarkable aspects of this graph is the shift of the peak wavelength of the spectrum that reaches the PV cell, compared to the solar spectrum. This effect is caused by the chromatic selectivity of the HOEs, which are designed to perform more efficiently around 800 nm. The shape of the spectral irradiance received by the thermal absorber is rather similar to the solar spectrum, except for the optimum wavelength range of the PV

cell.

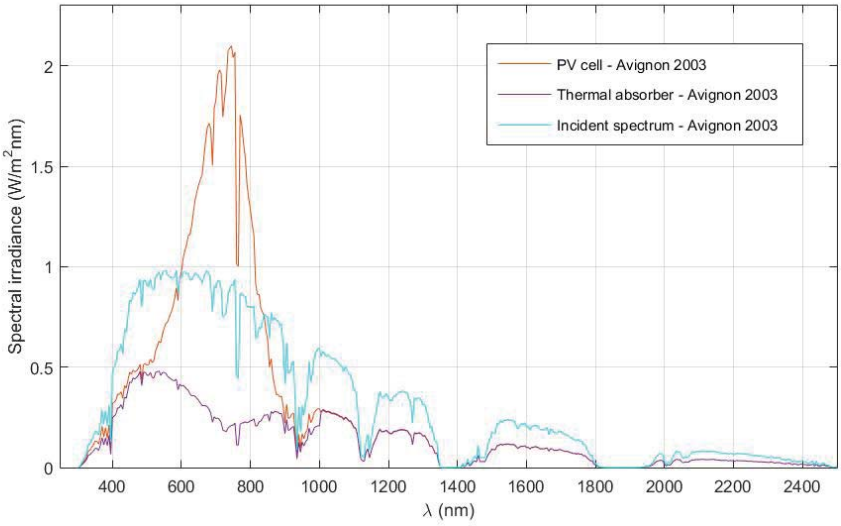

Figure 7. Average spectral irradiance at the entrance of the system, at the PV cell and at the thermal absorber at both locations.

The electrical energy produced by the HCPVT module expressed in terms of the PV cell area outperforms clearly the one delivered by the reference PVT system as it can be observed in Figure 8 a. More specifically the productions are 275.8 kWh/m^2 and 144.8 kWh/m^2 for the HCPVT and the reference PVT respectively. These values denote a mean effective optical concentration of about 2 for the whole spectrum where the PV cell is sensitive. In addition, figure 8b represents the results in a more widespread manner for PV systems that is in terms of the kilowatt pic (kWp). Conversely, in this case the energy values are the opposite: the reference system delivers almost twice the electric energy than the HCPVT (563.3 vs 296.4 kWh/kWp). This behavior is attributed to the low annual efficiency achieved by the concentrating system for all the spectral response bandwidth of the PV cell (43%) and it is a key indicator that further research in the optical design should be conducted to increase the average optical efficiency and therefore to obtain either similar or higher electrical yield values than in the reference module. On the other hand, it is worthy to mention that in terms of environmental impact the ten times reduction of the PV cell area, even the production to be the half than for the reference case in terms of kWp, reduces considerable the impact of the system as polymeric materials (used for the lenses) present in most of the cases and with all the particularities of each environmental indicator a much lower impact (Lamnatou et al., 2016).

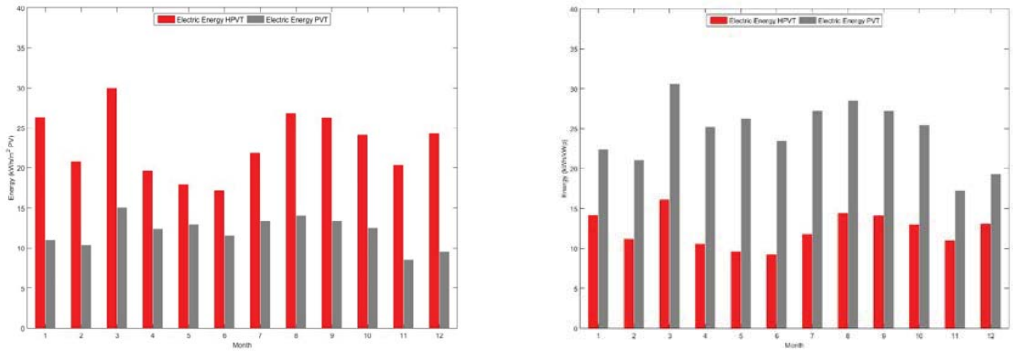

Figure 8. Electric energy output of the HCPVT system (grey bars) and the PVT system (red bars) along the year, expressed in terms of kWh/m^2 (left) and kWp (right).

The thermal energy output in both systems is quite simimilar, as it can be seen in Figure 9, reporting annual values of 250.4 and 294.2 kWh/m^2 of thermal collector area for the HCPVT and the reference PVT respectively. Therefore, the system proposed reports satisfactory values with respect to the thermal energy, however, concerning the electrical production further research is necessary not only from the energetical point of view but also considering environmental aspects.

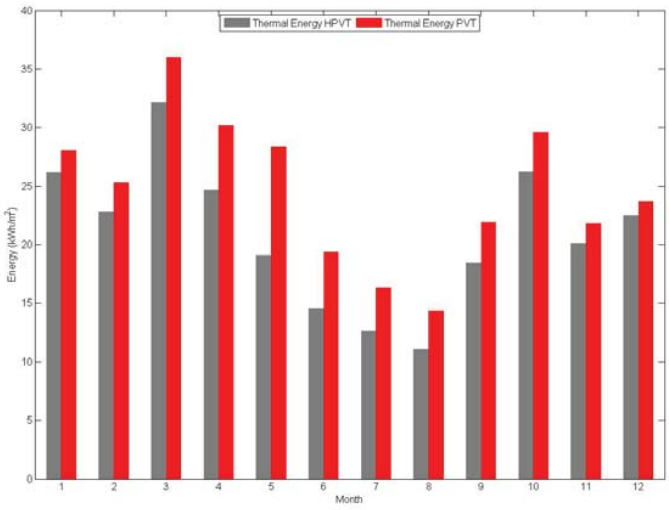

Fig 9. Thermal energy output of the HCPVT system (grey bars) and the PVT system (red bars) along the year.

5. Conclusions

A building-integrated holographic concentrating photovoltaic-thermal system has been designed and simulated. The module has been placed on the blinds of a solar louvre, which track the solar altitude movement of the sun along the day, on a south-oriented façade.

The direct normal irradiance solar spectra along one year have been calculated with the SMARTS radiative model, utilizing AERONET atmospheric parameters to test the concentrating system proposed under different spectral conditions. These spectra have been verified with direct irradiance measurements obtained from the Baseline Surface Radiation Network (BSRN), which proved the high accuracy of the simulations.

The behavior of the holographic concentrator, based on two holographic cylindrical lenses, was simulated by means of a ray-tracing algorithm. It concentrates toward the cell mainly its optimal wavelength range and also distributes the rest of the spectral irradiance on the thermal absorber, reaching a total optical efficiency. The annual average optical efficiency obtained is 43.0%.

A MATLAB-TRNSYS coupling was implemented to run simultaneously the optical, the thermal and the electrical simulations.

In the comparative study with respect to a reference photovoltaic-thermal conventional module installed with the same characteristics as the concentrating one, a similar thermal output was observed (~15% difference) but the electrical energy delivered by the reference module doubled the electricity production of the concentrating one (563.3 vs 296.4 kWh/kWp)

A future work of the present study is the improvement of the optical design to achieve higher mean optical efficiencies to obtain better electrical efficiencies mainly. In addition, environmental criteria should be considered to adequately estimate the differential performance of the holographic concentrator proposed.

6. References

Aerosol Robotic Network (AERONET) [WWW Document], n.d. URL http://aeronet.gsfc.nasa.gov/ (accessed 10.14.15).

Amrizal, N., Chemisana, D., Rosell, J.I., 2013. Hybrid photovoltaic–thermal solar collectors dynamic modeling. Appl. Energy 101, 797–807. doi:10.1016/j.apenergy.2012.08.020

Bañares-Palacios, P., Álvarez-Álvarez, S., Marín-Sáez, J., Collados, M.-V., Chemisana, D., Atencia, J., 2015. Broadband behavior of transmission volume holographic optical elements for solar concentration. Opt. Express 23, A671–A681. doi:10.1364/OE.23.00A671

Berneth, H., Bruder, F.-K., Fäcke, T., Jurbergs, D., Hagen, R., Hönel, D., Rölle, T., Walze, G., 2014. Bayfol HX photopolymer for full-color transmission volume Bragg gratings. SPIE Photonics West 2014-OPTO

Optoelectron. Devices Mater. 9006, 900602. doi:10.1117/12.2038399

Castillo, J.E., 2011. Thermal effects of the extended holographic regions for holographic planar concentrator. J. Photonics Energy 1, 15504. doi:10.1117/1.3569118

Castro, J.M., Zhang, D., Myer, B., Kostuk, R.K., 2010. Energy collection efficiency of holographic planar solar concentrators. Appl. Opt. 49, 858. doi:10.1364/AO.49.000858

Chan, N.L.A., Brindley, H.E., Ekins-Daukes, N.J., 2014. Impact of individual atmospheric parameters on CPV system power, energy yield and cost of energy. Prog. Photovoltaics Res. Appl. 22, 1080–1095. doi:10.1002/pip.2376

Chander, S., Purohit, A., Sharma, A., Nehra, S.P., Dhaka, M.S., 2015. A study on photovoltaic parameters of mono-crystalline silicon solar cell with cell temperature. Energy Reports 1, 104–109. doi:10.1016/j.egyr.2015.03.004

Chemisana, D., Collados, M.V., Quintanilla, M., Atencia, J., 2013. Holographic lenses for building integrated concentrating photovoltaics. Appl. Energy 110, 227–235. doi:10.1016/j.apenergy.2013.04.049

Collados, M.V., Chemisana, D., Atencia, J., 2016. Holographic solar energy systems: The role of optical elements. Renew. Sustain. Energy Rev. 59, 130–140. doi:10.1016/j.rser.2015.12.260

Directive 2010/31/EU of the European Parliament and of the Council of 19 May 2010 on the energy performance of buildings., 2010. . European Parliament, Strasbourg, France.

Froehlich, K., Wagemann, E.U., Frohn, B., Schulat, J., Stojanoff, C.G., 1993. Development and fabrication of a hybrid holographic solar concentrator for concurrent generation of electricity and thermal utilization, in: Lampert, C.M. (Ed.), Proceedings of SPIE. San Diego, USA, pp. 311–319. doi:10.1117/12.161971

Gueymard, C.A., 2001. Parameterized transmittance model for direct beam and circumsolar spectral irradiance. Sol. Energy 71, 325–346. doi:10.1016/S0038-092X(01)00054-8

Hecht, E., 1998. Optics. Addison Wesley.

Holben, B.N., Eck, T.F., Slutsker, I., Tanré, D., Buis, J.P., Setzer, A., Vermote, E., Reagan, J.A., Kaufman, Y.J., Nakajima, T., Lavenu, F., Jankowiak, I., Smirnov, A., 1998. AERONET—A Federated Instrument Network and Data Archive for Aerosol Characterization. Remote Sens. Environ. 66, 1–16. doi:10.1016/S0034-4257(98)00031-5

Iurevych, O., Gubin, S., Dudeck, M., 2012. Combined receiver of solar radiation with holographic planar concentrator. IOP Conf. Ser. Mater. Sci. Eng. 29, 12016. doi:10.1088/1757-899X/29/1/012016

Kogelnik, H., 1969. Coupled wave theory for thick hologram gratings. Bell Syst. Tech. J. 48, 2909–2947. doi:10.1002/j.1538-7305.1969.tb01198.x

Lamnatou, C., Baig, H., Chemisana, D., Mallick, T.K., 2016. Environmental assessment of a building-integrated linear dielectric-based concentrating photovoltaic according to multiple life-cycle indicators. J. Clean. Prod. 131, 773–784. doi:10.1016/j.jclepro.2016.04.094

Ludman, J.E., 1982. Holographic solar concentrator. Appl. Opt. 21, 3057–3058. doi:10.1364/AO.21.003057

Ludman, J.E., Riccobono, J., Semenova, I. V., Reinhand, N.O., Tai, W., Li, X., Syphers, G., Rallis, E., Sliker, G., Martín, J., 1997. The optimization of a holographic system for solar power generation. Sol. Energy 60, 1–9. doi:10.1016/S0038-092X(96)00148-X

Marín-Sáez, J., Atencia, J., Chemisana, D., Collados, M.-V., 2016a. Characterization of volume holographic optical elements recorded in Bayfol HX photopolymer for solar photovoltaic applications. Opt. Express 24, A720. doi:10.1364/OE.24.00A720

Marín-Sáez, J., Chemisana, D., Moreno, Á., Riverola, A., Atencia, J., Collados, M.-V., 2016b. Energy Simulation of a Holographic PVT Concentrating System for Building Integration Applications. Energies 9, 577. doi:10.3390/en9080577

Marion, B., 2002. A method for modeling the current-voltage curve of a PV module for outdoor conditions. Prog. Photovoltaics Res. Appl. 10, 205–214. doi:10.1002/pip.403

Menoufi, K., Chemisana, D., Rosell, J.I., 2013. Life Cycle Assessment of a Building Integrated Concentrated Photovoltaic scheme. Appl. Energy 111, 505–514. doi:10.1016/j.apenergy.2013.05.037

Schüco [WWW Document], n.d. URL www.schueco.com (accessed 5.27.16).

Solar and Wind Energy Resource Assessment (SWERA) [WWW Document], n.d. URL https://maps.nrel.gov/swera (accessed 5.27.16).

Sunways [WWW Document], n.d. URL www.sunways.eu (accessed 1.1.13).

Syms, R.R.A., 1985. Vector Effects in Holographic Optical Elements. Opt. Acta Int. J. Opt. 32, 1413–1425. doi:10.1080/713821663

Vorndran, S., Russo, J.M., Wu, Y., Gordon, M., Kostuk, R., 2015. Holographic diffraction-through-aperture spectrum splitting for increased hybrid solar energy conversion efficiency. Int. J. Energy Res. 39, 326–335. doi:10.1002/er.3245

World Radiation Monitoring Center – Baseline Surface Radiation Network homepage. [WWW Document], n.d. URL http://bsrn.awi.de/ (accessed 5.27.16).

Xia, X.W., Parfenov, A. V., Aye, T.M., Shih, M.-Y., 2011. Efficient hybrid electric and thermal energy generation, in: VanSant, K., Sherif, R.A. (Eds.), Proceedings of SPIE. San Diego, USA, p. 81080F. doi:10.1117/12.894166

Xiao, C., Yu, X., Yang, D., Que, D., 2014. Impact of solar irradiance intensity and temperature on the performance of compensated crystalline silicon solar cells. Sol. Energy Mater. Sol. Cells 128, 427–434. doi:10.1016/j.solmat.2014.06.018

Zhang, D., Castro, J.M., Kostuk, R.K., 2011. One-axis tracking holographic planar concentrator systems. J. Photonics Energy 1, 15505. doi:10.1117/1.3590943

Zhang, D., Gordon, M., Russo, J.M., Vorndran, S., Kostuk, R.K., 2013. Spectrum-splitting photovoltaic system using transmission holographic lenses. J. Photonics Energy 3, 34597. doi:10.1117/1.JPE.3.034597